Direct Evidence for Nitrogen Ligation to the High Stability Semiquinone Intermediate in *Escherichia coli* Nitrate Reductase A[*]

Stéphane Grimaldi[‡1], **Rodrigo Arias-Cartin**[§], **Pascal Lanciano**[‡2], **Sevdalina Lyubenova**[¶], **Burkhard Endeward**[¶], **Thomas F. Prisner**[¶], **Axel Magalon**[§], and **Bruno Guigliarelli**[‡]

From the ‡*Unité de Bioénergétique et Ingénierie des Protéines (UPR9036) and* §*Laboratoire de Chimie Bactérienne (UPR9043), Institut de Microbiologie de la Méditerranée, CNRS and Aix-Marseille Université, 31, chemin Joseph Aiguier, 13402 Marseille Cedex 20, France and the* ¶*Institut für Physikalische und Theoretische Chemie, J. W. Goethe Universität, Max-von-Laue-Strasse 7, 60438 Frankfurt, Germany*

The membrane-bound heterotrimeric nitrate reductase A (NarGHI) catalyzes the oxidation of quinols in the cytoplasmic membrane of *Escherichia coli* and reduces nitrate to nitrite in the cytoplasm. The enzyme strongly stabilizes a menasemiquinone intermediate at a quinol oxidation site (Q_D) located in the vicinity of the distal heme b_D. Here molecular details of the interaction between the semiquinone radical and the protein environment have been provided using advanced multifrequency pulsed EPR methods. ^{14}N and ^{15}N ESEEM and HYSCORE measurements carried out at X-band ($\sim$9.7 GHz) on the wild-type enzyme or the enzyme uniformly labeled with ^{15}N nuclei reveal an interaction between the semiquinone and a single nitrogen nucleus. The isotropic hyperfine coupling constant $A_{iso}(^{14}N)$ $\sim$0.8 MHz shows that it occurs via an H-bond to one of the quinone carbonyl group. Using ^{14}N ESEEM and HYSCORE spectroscopies at a lower frequency (S-band, $\sim$3.4 GHz), the ^{14}N nuclear quadrupolar parameters of the interacting nitrogen nucleus ($\kappa = 0.49$, $\eta = 0.50$) were determined and correspond to those of a histidine N_δ, assigned to the heme b_D ligand His-66 residue. Moreover S-band ^{15}N ESEEM spectra enabled us to directly measure the anisotropic part of the nitrogen hyperfine interaction ($T(^{15}N) = 0.16$ MHz). A distance of $\sim$2.2 Å between the carbonyl oxygen and the nitrogen could then be calculated. Mechanistic implications of these results are discussed in the context of the peculiar properties of the menasemiquinone intermediate stabilized at the Q_D site of NarGHI.

In the absence of oxygen and in the presence of nitrate, *Escherichia coli* induces the production of two energy-converting enzymes: formate dehydrogenase-N (FdnGHI) and dissimilatory nitrate reductase A (NarGHI).[3] These two complexes cooperate in generating a proton motive force through the redox loop mechanism as originally envisaged by Peter Mitchell in his chemiosmotic hypothesis (1). The separation of positive and negative charges across the cytoplasmic membrane is achieved through electron transfer from the formate oxidation site in the periplasm to the nitrate reduction site located on the cytoplasmic space with mena- or ubiquinone/quinol cycling between them (2, 3).

The heterotrimeric NarGHI complex is composed of (i) a nitrate-reducing subunit NarG containing a Mo-*bis*-MGD cofactor (Moco) and a [4Fe-4S] cluster FeS0 with unusual His coordination (4, 5), (ii) an electron transfer subunit NarH carrying four FeS clusters (6), and (iii) a membrane anchor subunit NarI containing two *b*-type hemes termed b_D and b_P to indicate their distal and proximal positions with respect to the nitrate-reducing site (7–9). These prosthetic groups define an electron transfer pathway from a periplasmically oriented quinol oxidation site (Q_D) to a cytoplasmically oriented nitrate reduction site.

Although considerable research has been devoted to nitrate reductase functioning, only partial information has been gained about the number, the structure, and the specificity of quinol binding sites within NarGHI. For instance, some studies have reported on mena- and ubiquinol analogue binding (10–20), whereas the molecular details of the interaction between natural quinols and NarGHI remain to be established.

Despite the absence of bound quinones in the available high resolution structures of NarGHI (7, 20), the crystal structure of the enzyme in complex with pentachlorophenol (PCP), an inhibitor of the quinol oxidase activity, has been determined (20). Based on mutagenesis data, biochemical analyses, and molecular modeling, a model of the Q_D quinol binding site has been proposed (20). In this working model, a quinone carbonyl group interacts with the protein via a hydrogen bond to a histidine residue (His-66), which is one of the axial ligands of heme b_D. Molecular modeling of a menaquinone in the PCP binding site suggested that the opposite carbonyl group could form a hydrogen bond to Lys-86 (20). Additionally, an elongated

---

1 To whom correspondence should be addressed. Tel.: 33-491-164-557; Fax: 33-491-164-097; E-mail: grimaldi@ifr88.cnrs-mrs.fr.
2 Present address: Dept. of Biology, Plant Science Institute, University of Pennsylvania, Philadelphia, PA 19104.

3 The abbreviations used are: NarGHI, membrane-bound heterotrimeric nitrate reductase A; EPR, electron paramagnetic resonance; Moco, molybdenum cofactor; ESEEM, electron spin echo envelope modulation; HYSCORE, hyperfine sublevel correlation; MSQ_D, menasemiquinone stabilized at the Q_D site of NarGHI; NQR, nuclear quadrupole resonance; ENDOR, electron nuclear double resonance; ESE, electron spin echo; DFT, density functional theory; PCP, pentachlorophenol; EFG, electric field gradient.

Q_D Site Semiquinone in the Nitrate Reductase

hydrophobic cavity where both hemes are exposed was proposed as a possible secondary quinone reactive site (7, 20).

We have shown that a semiquinone (SQ) intermediate can be stabilized in wild-type NarGHI by redox titration monitored by EPR spectroscopy (18). The radical cannot be detected in the presence of an excess of 2-*n*-nonyl-4-hydroxyquinoline-*N*-oxide (NQNO), a menaquinol analogue that binds in the vicinity of the distal heme. The radical has a midpoint potential $E_{m,7.5 \ (Q/QH2)} \sim -90$ mV, characteristic of a menasemiquinone (MSQ) species. Remarkably, the MSQ stability constant measured in NarGHI ($K_s \sim 70$) is the largest measured so far in respiratory complexes stabilizing semiquinone species (21–23). Interestingly, although this semiquinone species is present in a mutant lacking the proximal heme b_P, it cannot be detected in variants lacking the distal heme or upon substitution of the surrounding Lys-86 residue by an Ala (NarGHI$_{K86A}$) (19). The latter variant exhibits a strong decrease in quinol oxidase activity whatever the tested quinol analogs are (19, 20). On the basis of these observations, we concluded that the menasemiquinone radical is located in the vicinity of heme b_D (hereafter referred to as MSQ$_D$) and that Lys-86 is required for its stabilization (19). However, the molecular factors responsible for the high MSQ$_D$ stabilization and the role of this stability during the enzyme mechanism remain to be elucidated.

Understanding the quinol oxidation mechanism by NarGHI requires identification of ligands for all three forms, Q, SQ, and QH$_2$. In particular, interactions between quinone carbonyl oxygen atoms and H-bond-donating amino acid residues have been suggested to be an important factor in determining the properties of bound semiquinones (24). In this work, the Q$_D$ quinol oxidation site of NarGHI was studied by high resolution EPR methods using the unpaired electron spin of the endogeneous MSQ$_D$ intermediate as a probe of its environment. High resolution pulsed EPR techniques such as ESEEM (electron spin echo envelope modulation) and its two-dimensional variant HYSCORE (hyperfine sublevel correlation) are powerful tools for probing the local environment of protein-bound radicals at the atomic level. In particular, they have been shown to be useful for detecting weak hyperfine interactions between nuclear spins of ^{14}N atoms and the unpaired electron spin of protein-bound semiquinones (24–31). Application of multifrequency techniques makes it possible to interpret the ESEEM features and to utilize them to reliably measure hyperfine and quadrupole interactions in orientationally disordered samples such as frozen protein (27, 32, 33). Nuclear quadrupole parameters can then be used to distinguish nitrogen originating from the peptide bond or from amino acid side chains (25, 27–31, 34–36).

In this work, S-band ($\sim$3 GHz) and X-band ($\sim$9 GHz) ESEEM/HYSCORE experiments were performed directly on *E. coli* membrane fractions containing overexpressed NarGHI. The use of native and uniformly ^{15}N-labeled proteins allow us to provide the first direct experimental evidence of nitrogen ligation to the MSQ bound within the Q$_D$ site of NarGHI in its natural environment. It is identified as the N$_\delta$ imidazole nitrogen of a histidine residue, most likely heme b_D ligand His-66.

EXPERIMENTAL PROCEDURES

Sample Preparation—Purified *E. coli* NarGHI-enriched membrane fractions were prepared as described in Ref. 19. ^{15}N uniformly labeled NarGHI was obtained after growth in M9 minimal medium (37) supplemented with Mohr salt (25 mg/liter), Na$_2$MoO$_4$ (220 ng/liter), and [^{15}N]NH$_4$Cl (1 g/liter). Glycerol (0.4% v/v) was used as a carbon source instead of glucose. Thiamine (10 mg/liter) and appropriate antibiotics were added before inoculation, and all cultures were performed at 37 °C under semi-anaerobic conditions.

Stabilization of the semiquinone at the Q$_D$ site was achieved through redox titrations under the same conditions as those used in our previous work (18). Redox potentials are given in the text with respect to the standard hydrogen electrode.

Multifrequency Pulsed EPR Experiments—X-band ($\sim$9 GHz) pulsed EPR experiments were performed using a Bruker EleXsys E580 spectrometer equipped with an Oxford Instruments CF 935 cryostat. S-band pulsed EPR experiments were carried out on a home-built pulsed S-band EPR spectrometer (27, 38) at a microwave frequency of $\sim$3.4 GHz, which corresponds to the resonance field $\sim$122 mT for paramagnetic species with a g-factor of $\sim$2.

For the two-pulse field sweep ESE (electron spin echo) spectra, the echo integral was recorded as a function of the magnetic field after a two-pulse Hahn-echo sequence ($\pi/2$ - 200 ns - π). In the one-dimensional three-pulse ESEEM experiment ($\pi/2$ - τ - $\pi/2$ - T- $\pi/2$), the intensity of the stimulated echo signal after the third pulse is recorded as a function of time, t, at constant time, τ. 2D-HYSCORE spectra were recorded using the sequence ($\pi/2$ - τ - $\pi/2$ - t_1 - π - t_2 - $\pi/2$), where the inverted three-pulse echo generated at a time τ after the last pulse is measured as a function of t_1 and t_2.

All ESEEM and HYSCORE spectra were recorded at a magnetic field corresponding to the maximum intensity of the MSQ$_D$ signal in the two-pulse field sweep ESE spectrum, where all orientations of the semiquinone with respect to the external magnetic field contribute, giving rise to powder ESEEM/HYSCORE spectra. Appropriate phase cycling procedures were applied in the stimulated echo and HYSCORE experiments to remove the unwanted echoes (39). Spectral processing of three-pulse and HYSCORE spectra was performed using Bruker Xepr software.

Relaxation decays were subtracted (fitting by polynomial functions) followed by zero-filling and tapering with a Hamming window, before Fourier transformation, which finally gives the spectrum in frequency domain. All spectra are shown in absolute value mode. HYSCORE spectra are presented as contour plots.

Hyperfine and Nuclear Quadrupole Interactions—A hyperfine coupling between a $S = \frac{1}{2}$ radical and a nucleus with nuclear spin value I consists in general of (i) the isotropic contribution $A_{iso} = 2\mu_0 g_e g_n \beta_e \beta_n \ \psi_0(0)^2/3h$ where $\psi_0(0)^2$ is the electron spin density at the nucleus, g_e and g_n are electron and nuclear g-factors, respectively, β_e and β_n are Bohr and nuclear magnetons, respectively, h is Planck's constant, and (ii) the anisotropic contribution described by the dipolar coupling ten-

sor $\tilde{T}$. In the point-dipole approximation $\tilde{T}$ has axial symmetry with principal values (A_{iso} - T, A_{iso} - T, A_{iso} + 2T),

$$T = \mu_0 g_e g_n \beta_e \beta_n / 4\pi h r^3 \qquad \text{(Eq. 1)}$$

where *r* is the distance between the nucleus and the electron.

The hyperfine couplings of different isotopes of the same element are proportional to a very good approximation to the corresponding g_n values. In this study, the parameter A_{iso} of the nitrogen interacting with the SQ was derived from X-band ^{14}N and ^{15}N ESEEM measurements while T was directly determined from S-band ^{15}N ESEEM.

A ^{14}N nucleus has a quadrupole moment that interacts with the electric field gradient (EFG) at the nucleus. The components of the EFG tensor are defined in its principal axis system and are ordered according to $q_{ZZ} \geq q_{YY} \geq q_{XX}$. This traceless tensor can then be fully described by only two parameters: (i) the ^{14}N nuclear quadrupole coupling constant $\kappa = e^2 q_{ZZ} Q/h$, where e is the charge of electron, Q is the nuclear electric quadrupole moment of the ^{14}N nucleus, (ii) the asymmetry parameter $\eta = q_{YY} - q_{XX}/q_{ZZ}$. κ is a measure of the strength of the interaction between the nuclear quadrupole moment and the EFG at the ^{14}N nucleus site due to anisotropic charge distribution in the system, whereas η is a measure of the deviation of the charge distribution from axial symmetry. κ and η are extremely sensitive to atomic and chemical bond arrangements and are excellent probes for the identification of bonding geometry and of the chemical group housing the nucleus. They can, therefore, be used for the identification and characterization of the ^{14}N atom. In this study, the parameters κ and η of the nitrogen interacting with MSQ$_D$ were derived using S-band ^{14}N ESEEM.

^{14}N and ^{15}N Powder ESEEM Spectra—Powder ESEEM spectra given by a frozen protein solution for $S = \frac{1}{2}$ interacting with a nucleus with $I = \frac{1}{2}$ (e.g. ^{15}N) and $I = 1$ (*e.g.* ^{14}N) have been extensively analyzed (40). For $I = \frac{1}{2}$, it has been shown that the relative magnitude of the hyperfine and nuclear Zeeman interactions determines the shape of the ESEEM spectra. In the case of an axial hyperfine tensor for $4\nu_I = 2A_{iso} + T$ known as "matching condition" (ν_I is the nuclear Larmor frequency), the ESEEM spectrum has a characteristic shape; *i.e.* it is characterized by two frequencies with a dominant narrow feature at $\nu_\alpha = 3T/4$ and a broad, weak one at $\nu_\beta \sim 2\nu_I$. A modest rhombicity of the hyperfine coupling influences the width but not the position of the intense low frequency line at ν_α. Thus the determination of T from this ESEEM frequency is not affected by the rhombicity of the hyperfine interaction (32).

For hyperfine couplings that deviate from the matching condition, the intensity and resolution of spectral features decreases significantly. For weak couplings $A_{iso} < 2\nu_I$ the main peaks are centered approximately at ν_I.

A ^{14}N nucleus interacting with an unpaired electron spin $S = \frac{1}{2}$ can produce up to six lines in an ESEEM spectrum. They correspond to the 6 nuclear transition frequencies between three nuclear energy sublevels in each of the two electron spin manifolds with $m_s = \pm \frac{1}{2}$. Because of their different dependence on orientation, not all transitions contribute equally to the spectra in ESEEM measurements of disordered samples (as in

the case of the frozen suspensions of NarGHI-enriched membrane fractions used in our experiments). The ESEEM spectrum expected for ^{14}N with predominantly isotropic hyperfine coupling constant A_{iso} is governed by the ratio between the effective nuclear frequency in each manifold $\nu_{ef\pm} = \nu_I \pm A_{iso}/2$, and the quadrupole coupling constant, κ.

If $\nu_{ef\pm}/\kappa \sim 0$, *i.e.* $A_{iso} \cong 2\nu_I$, the nuclear Zeeman and hyperfine splitting cancel in one electron spin manifold. This situation is thus called "cancellation condition." Therefore, the three nuclear frequencies from this manifold are close to the pure nuclear quadrupole resonance frequencies of ^{14}N transitions and are given by the relationships in Equation 2,

$$\nu_+ = \kappa(3 + \eta); \quad \nu_- = \kappa(3 - \eta); \quad \nu_0 = 2\kappa\eta \qquad \text{(Eq. 2)}$$

In this case, three sharp lines at the frequencies given by Equation 2 are present in the powder ESEEM spectra with the simple additive relationship $\nu_- + \nu_0 = \nu_+$. Pure quadrupole frequencies can even be observed if cancellation is not exact, as long as the condition in Equation 3,

$$|A_{iso} - 2\nu_I| < 4\kappa/3 \qquad \text{(Eq. 3)}$$

is fulfilled (33). When $\nu_{ef\pm}/\kappa > 1$, only a single line without pronounced orientation dependence from each corresponding manifold is expected. It is actually a double-quantum transition line $\Delta m_I = 2$ giving maximum intensity at a frequency well described by Equation 4,

$$\nu_{dq\pm} = 2(\nu_{ef\pm}^2 + c)^{1/2} \qquad \text{(Eq. 4)}$$

where

$$c = \kappa^2(3 + \eta^2) \qquad \text{(Eq. 5)}$$

The two single quantum transitions usually do not show any resolved peaks because of significant orientation dependence from quadrupole interaction. The relative strength of the hyperfine coupling and the Zeeman nuclear frequency can be varied by changing the frequency of the microwave radiation used for the ESEEM/HYSCORE measurements. In this work, this strategy was applied to reach the cancellation condition (^{14}N) or the matching condition (^{15}N) for the detected nucleus at S-band frequencies.

RESULTS

X-band Pulsed EPR of Native and ^{15}N-Labeled NarGHI—Our previous studies revealed that an EPR-detectable mena-semiquinone intermediate can be generated in the wild-type nitrate reductase A by direct chemical reduction of purified *E. coli* NarGHI-enriched membrane fractions (18), the maximal SQ concentration being reached at a redox potential around −100 mV at pH 7.5 (18). To specifically characterize by pulsed EPR the interaction of the semiquinone with nearby nitrogen atoms, MSQ$_D$ was generated either in unlabeled or in uniformly ^{15}N-labeled protein sample (see "Experimental Procedures"). In both preparations issued from bacteria grown in a modified M9 minimal medium, the semiquinone concentration relative to the [3Fe-4S] cluster ($\sim$6–8%) and the quinol:
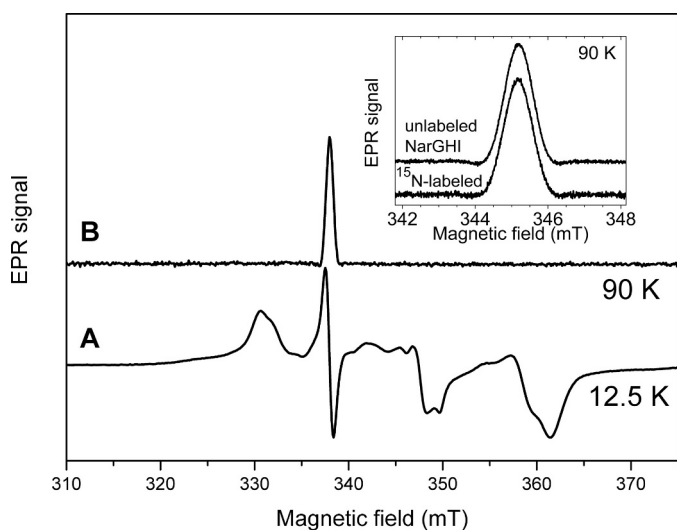
Q_D Site Semiquinone in the Nitrate Reductase

FIGURE 1. **X-band EPR spectra of MSQ$_D$ in *E. coli* membrane fractions containing overexpressed NarGHI.** *A*, continuous wave EPR spectrum of a sample redox poised at ~ -105 mV and measured at 12.5 K. *B*, two-pulse field sweep ESE spectra of the same sample recorded at 90 K. Other experimental conditions were: microwave frequency 9.4695 GHZ (*A*), 9.6912 GHz (*B*), τ 200 ns, $\pi/2$, and π pulse lengths 12 and 24 ns, respectively, microwave power 1 milliwatt (*A*), field modulation parameters: 0.5 mT at 100 kHz. Because of differences in experimental microwave frequency used for continuous wave and pulsed EPR experiments, magnetic field values of spectrum B were corrected allowing direct comparison with spectrum A. The *inset* shows two-pulse field sweep ESE spectra of MSQ$_D$ in unlabeled (*top*) and uniformly ^{15}N-labeled (*bottom*) NarGHI recorded at 90 K.

nitrate oxidoreductase activity were identical to those measured in a preparation obtained from bacteria grown in Terrific Broth medium.

Although several FeS clusters are paramagnetic at -100 mV and give signals in the spectral region where MSQ$_D$ appears ($g \sim 2.0$) (Fig. 1*A*) (41), the radical can be specifically detected without contamination from the other centers by exploiting differences in the temperature dependence of the relaxation time of these species. Thus, at 90 K, the FeS clusters are too fast relaxing to contribute to the EPR spectrum. This is illustrated in Fig. 1*B*, which shows the two-pulse field-sweep ESE spectrum, measured at 90 K, of membrane fractions containing overproduced native NarGHI (with the 99.63% of ^{14}N natural abundance) (Fig. 1*B* and *inset*, *top*) or the ^{15}N-labeled protein (*inset*, *bottom*). In both samples, the single line of SQ is the only one present and has identical line width ~ 0.8 mT (see *inset* in Fig. 1). This is expected because the major contributions to the observed line width are (i) unresolved g-tensor anisotropy and (ii) unresolved hyperfine couplings to the many protons in the vicinity of the radical (18). The line width is identical to that of the CW EPR spectrum of the native enzyme (18). In particular, magnetic interactions smaller than 0.5 mT (in field units) are not resolved on these spectra.

X-band HYSCORE—To resolve weak ^{14}N or ^{15}N magnetic interactions with the semiquinone, high resolution pulsed EPR methods were used at 90 K. Three-pulse ESEEM spectra of the radical have been recorded and have revealed low frequency modulations of the electron spin echo decay indicative of a hyperfine interaction with nuclei having low gyromagnetic ratio such as ^{14}N (data not shown). To facilitate the interpretation of the spectra and to increase their resolution, ^{14}N and ^{15}N
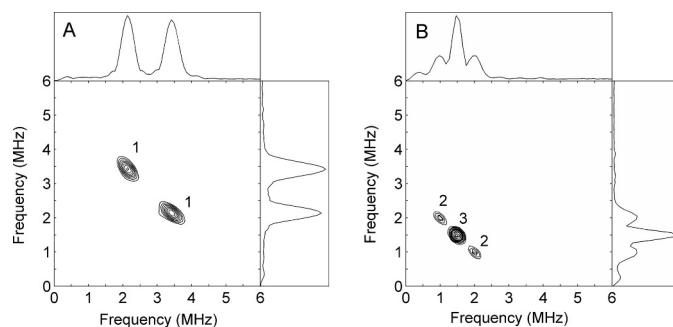

FIGURE 2. **X-band HYSCORE spectra of MSQ$_D$ in NarGHI.** Redox-poised samples (~ -105 mV) issued from membrane fractions containing overexpressed unlabeled NarGHI (*A*) or uniformly ^{15}N-labeled NarGHI (*B*) were used. Temperature was 90 K, microwave frequency was 9.6540 GHz, magnetic field was 343.3 mT. For spectrum A, the durations of the $\pi/2$ and π pulses were 12 and 24 ns, respectively, with equal amplitude, while both durations were equal to 12 ns for spectrum B, and the π pulse amplitude was optimized for maximal echo inversion. 256 points were recorded in each dimension for $\tau =$ 136 ns (*A*) and $\tau =$ 204 ns (*B*). t_1 and t_2 were incremented in steps of 16 ns (*A*) or 20 ns (*B*) from their initial value.

HYSCORE spectra were recorded using different τ values to avoid peak suppression effects (*i.e.* blind spots) (39). A typical ^{14}N HYSCORE spectrum of MSQ$_D$ showing the low frequency part of the two-dimensional plot after data processing is displayed in Fig. 2*A*. It exhibits two intense off-diagonal crosspeaks **1** in the ($++$) quadrant, correlating nuclear transition frequencies at 2.1 and 3.4 MHz.

A HYSCORE spectrum of MSQ$_D$ measured with the ^{15}N-labeled enzyme is depicted in Fig. 2*B*. The spectrum contains a prominent peak **3** on the diagonal at the ^{15}N Zeeman frequency ($\nu_I(^{15}N) = 1.48$ MHz) and two crosspeaks **2** centered symmetrically with respect to this diagonal peak, with maxima at frequencies 0.98 and 2.05 MHz. The loss of crosspeaks **1** observed in unlabeled NarGHI is thus related with the appearance of crosspeaks **2** in the ^{15}N-labeled protein. No other correlation could be resolved in HYSCORE spectra measured at 90 K using other τ values. These observations allow an unequivocal assignment of crosspeaks **1** & **2** to a single nitrogen nucleus. Their circular contour line shape suggests that the corresponding nuclear transitions are weakly anisotropic. A ^{15}N nucleus has a spin ½, and so does not possess the nuclear quadrupole moment that affects a ^{14}N nucleus (I = 1). Thus, a ^{15}N nitrogen hyperfine coupling of ~ 1.1 MHz can be directly estimated by reading the splitting between crosspeaks **2**. The intense diagonal peak **3** is not seen in ^{14}N spectra. It is contributed by all the other ^{15}N nuclei around the SQ, which are involved only in weak interactions with the unpaired electron (27, 29, 34, 42).

The observation of only two narrow crosspeaks **1** correlating ^{14}N nuclear transition frequencies belonging to opposite electron spin manifolds indicates a ^{14}N hyperfine interaction with both ratios $\nu_{ef\pm}/\kappa > 1$. These peaks could, therefore, be assigned to the double-quantum transitions $\nu_{dq+} = 3.4$ MHz and $\nu_{dq-} = 2.1$ MHz. Application of Equations 4 and 5 to these with $\nu_I(^{14}N) = 1.06$ MHz provides values of $A_{iso}(^{14}N) = 0.8$ MHz and c $= 0.77$ MHz^2. The former is in excellent agreement with the value of $A_{iso}(^{15}N) \sim 1.1$ MHz determined from the ^{15}N HYSCORE spectrum that leads to a value $A_{iso}(^{14}N) \sim 0.76$ MHz when rescaled to the ^{14}N nucleus. For these values of $A_{iso}(^{14}N)$
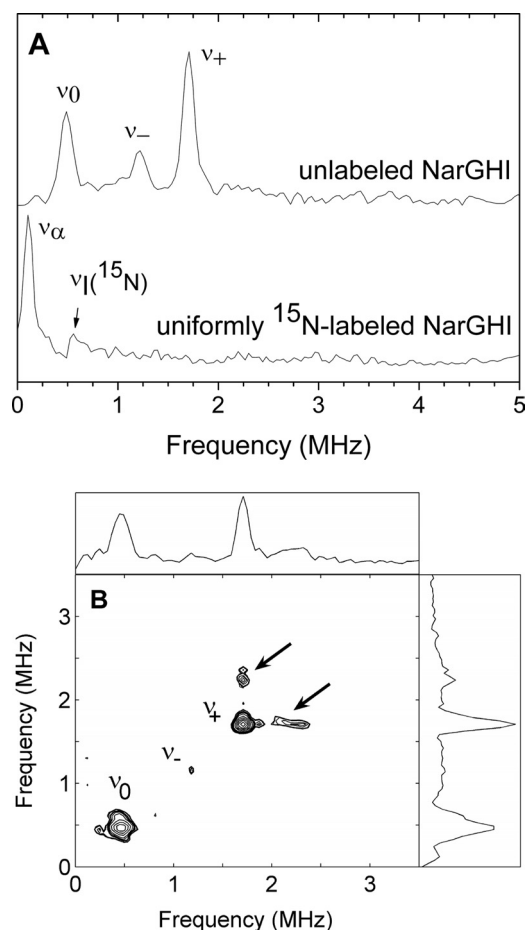
FIGURE 3. **S-band ESEEM/HYSCORE spectra of MSQ$_D$ in NarGHI.** *A*, three-pulse ^{14}N and ^{15}N ESEEM spectra of MSQ$_D$ in *E. coli* membrane fractions containing overexpressed unlabeled (*A*, *top* and *B*) and uniformly ^{15}N-labeled (*A*, *bottom*) NarGHI. The echo envelope was obtained by varying the time between the second and third microwave pulses, with an increment of 28 ns. A ^{14}N HYSCORE spectrum of MSQ$_D$ is shown in *B*. Correlations between the double-quantum nuclear frequencies from each manifold are indicated by *arrows*. Experimental conditions: temperature, 90 K; microwave frequency, 3.4155 GHz; magnetic field value, 122.2 mT; $\pi/2$ and π pulses lengths, 24 ns and 48 ns, respectively. Spectra were recorded with time $\tau = 172$ ns between first and second microwave pulses. For the HYSCORE spectrum, t_1 and t_2 were incremented in steps of 48 ns from their initial value, and 256 points were recorded in each dimension.

and $\nu_I(^{14}\text{N})$, the κ value must then satisfy the condition $\kappa < 0.66$ (Equation 3).

S-band ESEEM and HYSCORE—Unambiguous determination of κ and η is required for complete description of the nuclear quadrupole interaction tensor and the assignment of the interacting nitrogen. These values can be determined from ESEEM experiments satisfying the cancellation condition for one of the electron spin manifold. For hyperfine coupling $A_{iso}(^{14}\text{N}) \sim 0.8$ MHz, the cancellation condition is reached at $\nu_I(^{14}\text{N}) \sim 0.4$ MHz, which requires an experiment at S-band with microwave frequency ~ 3 GHz. Fig. 3*A* (*top*) displays a representative S-band three-pulse ESEEM spectrum of MSQ$_D$ in native NarGHI. Three sharp peaks are observed at frequencies 0.49, 1.22, and 1.71 MHz. The additive relationship satisfied by these frequencies ($\nu_+ = \nu_0 + \nu_-$) as well as the typical increase in the electron spin echo envelope modulation depth measured in the time-domain spectrum (not shown) reflect the

situation where the hyperfine coupling is nearly equal to twice the nuclear Larmor frequency. This allows for an immediate assignment of the narrow peaks to three nuclear quadrupole interaction frequencies from the manifold with $\nu_{ef^-} \sim 0$ and thus the determination of the nuclear quadrupole interaction tensor parameters. Applications of Equation 2 using $\nu_0 = 0.49$ MHz, $\nu_- = 1.22$ MHz, and $\nu_+ = 1.71$ MHz lead to $\kappa = 0.49$ MHz and $\eta = 0.50$. The corresponding calculated value of $c = 0.78$ MHz^2 using Equation 5 is then fully consistent with our assignment of the nuclear frequencies measured on the X-band ^{14}N HYSCORE spectrum and with the analytic procedure used. The double-quantum transition of the opposite manifold is difficult to detect in the one-dimensional S-band ^{14}N ESEEM spectra taken at several τ values (Fig. 3*A*, *top* and data not shown). It is however expected to have a broader shape because of combined hyperfine and nuclear quadrupole interaction anisotropies. From Equation 4, it is predicted to appear at about ~ 2.3 MHz. We were however able to detect crosspeaks having an elongated shape in the S-band ^{14}N HYSCORE spectrum of MSQ$_D$ in native NarGHI, correlating the two double-quantum nuclear frequencies from each manifold at 1.71 and ~ 2.3 MHz (Fig. 3*B*), showing the full consistency of our assignment.

The lack of extended anisotropic contours in the crosspeaks along the line normal to the diagonal of the X-band ^{14}N and ^{15}N HYSCORE spectra limits the accuracy of the determination of the anisotropic part of the hyperfine tensor. To overcome this limitation and gain information on the location of the interacting nucleus, S-band ESEEM experiments have been carried out on ^{15}N-labeled NarGHI to fulfill the matching condition for the interacting nitrogen nucleus. In this case, the spectrum is not complicated by the contribution of the nuclear quadrupole interaction and allows straightforward evaluation of the anisotropic part of the hyperfine interaction. Indeed, our previous measurement of $A_{iso}(^{15}\text{N}) = 1.07$ MHz implies that the condition $A_{iso}(^{15}\text{N})/2 \sim \nu_I(^{15}\text{N})$ is valid (at 122.2 mT, $\nu_I(^{15}\text{N}) \sim 0.57$ MHz). Fig. 3*A* (*bottom*) shows a representative frequency domain three-pulse ESEEM spectrum of MSQ$_D$ in ^{15}N-labeled NarGHI recorded at 3.4 GHz. The dominating feature is a peak at 0.12 MHz that we assign to the frequency ν_α of the ^{15}N nucleus. A second peak is present at frequency ~ 0.56 MHz, which matches the ^{15}N Larmor frequency. It arises from weakly coupled distant ^{15}N nuclei, as previously discussed. The partner of the line ν_α is not detected in our S-band ESEEM spectra taken at several τ values. This is due to its expected low intensity (39) and the limited achievable signal-to-noise ratio. According to this analysis, we have $3 \text{ T}(^{15}\text{N})/4 \sim 0.12$ MHz which yields $\text{T}(^{15}\text{N}) \sim 0.16$ MHz or $\text{T}(^{14}\text{N}) \sim 0.11$ MHz when rescaled to ^{14}N nucleus. This value is in full agreement with our previous analysis of ^{14}N and ^{15}N HYSCORE spectra.

DISCUSSION

Characteristics of the Interaction and Assignment of the Interacting Nitrogen—The characteristic changes observed in the HYSCORE spectra of the menasemiquinone intermediate in NarGHI upon isotopic substitution of ^{14}N by ^{15}N demonstrate that the low frequency modulations arise from a single nitrogen nucleus coupled to the semiquinone. The use of S-band ESEEM/HYSCORE allowed us to accurately measure the

parameters of this interaction. The existence of a nonzero isotropic hyperfine coupling constant A_{iso} (^{14}N) for the interacting nitrogen indicates that unpaired electron spin density is transferred from the semiquinone onto this nucleus. The value A_{iso} (^{14}N) = 0.8 MHz, obtained from HYSCORE spectra, is determined mainly by the unpaired spin density in the nitrogen atom 2s orbital. It corresponds to a small delocalization of spin density $\rho_S \sim 0.4 \times 10^{-3}$ in this orbital (43). This is indicative of the existence of an atomic bridge between the semiquinone and the ^{14}N nucleus. The only likely mechanism for such a transfer is via a hydrogen bond between one of the SQ oxygens and this nitrogen. This result is supported by the detection of at least one exchangeable proton strongly coupled to MSQ_D by HYSCORE and ENDOR, visualized by substitution of H_2O by D_2O in redox-poised samples of *E. coli* NarGHI.[4]

The dipole-dipole interaction responsible for the anisotropic hyperfine interaction of the interacting nucleus is determined by the interspin distance and by the fraction of the electron spin density, which interacts with the nuclear spin. The distance between the coupled nitrogen and the semiquinone can be roughly estimated by using Equation 1. Assuming that the interaction occurs via an H-bond, it is probable that the coupling is dominated by the oxygen-nitrogen distance. Spin densities ranging from 0.19 to 0.23 on the oxygen atoms of semiquinones have been previously measured using ^{17}O-labeled quinones in alcoholic solvent (44) or in bacterial reaction centers (24). Substitution of these values into Equation 1 then gives r_{O-N} = 2.23 ± 0.13 Å, which is a rough estimate of the O-N distance.

For the assignment of the nitrogen atom, we rely on comparison of the ^{14}N nuclear quadrupole resonance parameters deduced from the present ESEEM data (κ = 0.49, η = 0.50) with those available in the literature from previous ESEEM studies of protein-bound semiquinones (25,27–31,34–36,45). Although experimental data are not available for all possible candidates, the κ parameter of the nitrogen interacting with the SQ stabilized in NarGHI is very close to the corresponding parameter measured for N_δ histidine nitrogens which possess values κ ~0.35–0.41 (Fig. 4). Corresponding η values are in the range 0.61–0.82. As the latter has been shown to be much more influenced by the geometry of the N-H bond than the κ parameter, the relatively small η value determined in this work may reflect a slightly different H-bonding pattern compared with that occurring for Q_A^- in bacterial reaction centers (30, 35, 36) or in photosystem II (25, 28). Interestingly, the quadrupole characteristics determined here for the ^{14}N nucleus interacting with MSQ_D in NarGHI are very close to the values calculated by Fritscher for an imidazole making a strong in-plane hydrogen bond with a water molecule (r_{O-N} ~2.7 Å) (46). Moreover, DFT calculations carried out on more realistic models of methylimidazole-benzosemiquinone complexes predict values of (κ, η) = (0.48, 0.61) for short (*i.e.* r_{O-N} = 2.75 Å) in plane hydrogen bond between both molecules. Thus, the good agreement between our experimental quadrupole coupling parameters and these theoretical predictions provide additional support for our
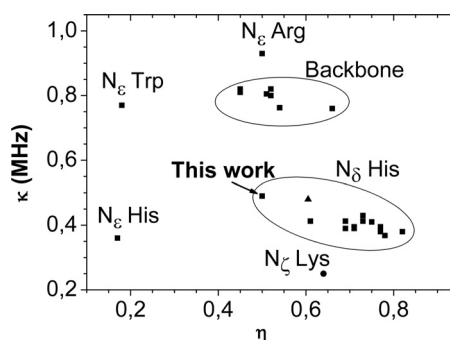
FIGURE 4. **Quadrupolar parameters of ^{14}N measured by ESEEM spectroscopy of membrane protein-bound semiquinones (■) or by ^{14}N NQR in amino acids (57) (●), or calculated by DFT for N_δ of methylimidazole-benzosemiquinone complexes (46) (▲).** The value of (κ, η) obtained in this work for the nucleus that interacts with MSQ_D in *E. coli* NarGHI is shown by an *arrow*. N_ϵ Trp at the phylloquinone site A_1 in photosystem I (31), N_ϵ His at the ubiquinone reduction site Q_i of bacterial bc_1 complex (27), N_ϵ Arg at the ubiquinone site Q_H in cytochrome bo_3 (34, 45), N_δ His and backbone nitrogen at the Q_A and Q_B sites of bacterial reaction centers (30, 35, 36) and photosystem II (25, 28, 29).
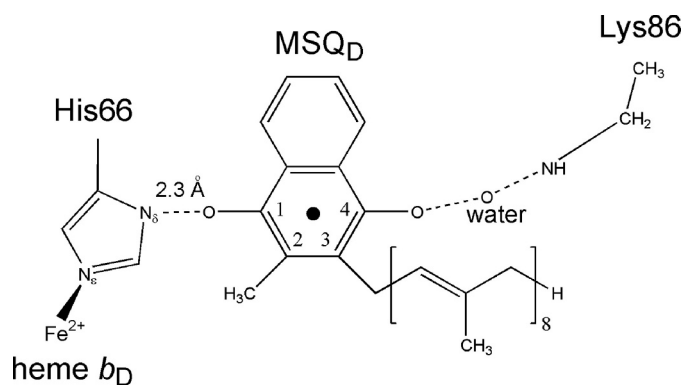

FIGURE 5. **A working model of the MSQ_D environment in *E. coli* NarGHI.** On the basis of our spectroscopic data and the structure of NarGHI co-crystallized with PCP, we propose that the N_δ of the His-66 imidazole H-bonds to the semiquinone O_1 while the N_ϵ coordinates the heme b_D iron. Whereas the nature of the ligand(s) to O4 remains unresolved, we propose that Lys-86 could be involved in hydrogen bonding to MSQ_D via a water molecule (see "Discussion"). The orientation of the quinone ring is taken to be identical to that obtained from molecular modeling of a menaquinone in the PCP-binding pocket by Bertero *et al.* (20).

assignment and for the involvement of this His nitrogen in hydrogen bonding to the semiquinone at the Q_D site.

In a previous work, we have clearly shown that the menasemiquinone radical of *E. coli* nitrate reductase A binds to the Q_D site, in the vicinity of the distal heme b_D (19). On the other hand, the crystal structure of the enzyme in complex with pentachlorophenol has been determined to 2.0 Å resolution (20). In the three-dimensional structure, the hydroxyl group of PCP is hydrogen bonded to one of the propionate groups of b_D and to N_δ-His-66. The r_{O-N} distance is 2.8 Å. Based on these structural data and given the fact that no other histidine residue is present in the Q_D site, we assign the interacting N_δ-His evidenced by our spectroscopic studies to His-66 (see Fig. 5). Thus, the presence of an H-bond to a histidine residue appears to be a common feature of both PCP and MSQ_D binding. This contrasts with the situation observed for the menaquinol oxidation site of the polysulfide reductase from *Thermus thermophilus* that has been recently characterized by cocrystallization experiments using the natural substrate menaquinone or the inhibitor PCP

(47). Although these compounds have been found in the same pocket, differences regarding the hydrogen bonding situation were evident.

Interestingly, the hyperfine coupling constants of the MSQ_D electron spin with the N_δ-His-66 nitrogen in NarGHI ($A_{iso}(^{14}N) = 0.8$ MHz, $T(^{14}N) \sim 0.11$ MHz) are very similar to the corresponding values $A_{iso}(^{14}N) = 0.8$ MHz, $T(^{14}N) \sim 0.1$–0.14 MHz) recently determined for the His nitrogen nucleus magnetically coupled to the ubisemiquinone anion Q_i^- stabilized at the quinone reduction site Q_i of the bc_1 complex from *Rhodobacter sphaeroides* (27, 48). This may reflect a similar mechanism of spin density transfer onto these nuclei. In both systems, it is likely that the presence and the redox state of the nearby heme (b_D in NarGHI, b_H in the bc_1 complex) plays a significant role in this mechanism of spin density transfer, as the heme is coordinated by a histidine ligand that interacts with the semiquinone formed in the Q site (49). It is noteworthy that in the redox-poised EPR samples used in this work for studying the MSQ_D properties, the b_D heme ($E_{m,7.5}$ $Fe^{2+}/Fe^{3+} \sim +20$ mV) is fully reduced, which mimics the catalytically relevant situation after that MQH_2 delivers one electron to the heme and forms the intermediate MSQ_D species. Similarly, the EPR-detectable Q_i^- intermediate in the bc_1 complex from *R. sphaeroides* has been suggested to be formed when heme b_H is reduced (48).

Further, systematic theoretical investigations of the influence of the hydrogen bond length r_{O-N} and of an in- or out-of-plane distortion of the bond geometry on the semiquinone-nitrogen hyperfine coupling constants would be useful to get a deeper insight into the mechanism of spin density transfer onto the histidine nitrogens coupled to Q_i^- and to MSQ_D. This will allow us to correlate the observed similar hyperfine couplings to a particular common bond geometry. Overall, the magnitude of the hyperfine interaction between MSQ_D and the N_δ-His-66 nitrogen indicates an overlap between the singly occupied molecular orbital of the radical and the His N_δ orbitals that is favorable for rapid electron transfer to heme b_D. However, the structural organization SQ-His-heme conserved in NarGHI and in the bc_1 complex does not appear critical by itself for tuning the radical stability. Indeed, the semiquinone stability constant K_S differs by three orders of magnitude in these complexes ($K_{S\ pH\ 7.5} \sim 70$ in NarGHI, $K_{S\ pH\ 7.7} \sim 10^{-2}$ in *R. sphaeroides bc_1* complex) (50). The high stabilization of MSQ_D in NarGHI is directly related to the redox potentials of the redox transitions MQH_2/MSQ ($E_{m,7.5} = -150$ mV) and MSQ/MQ ($E_{m,7.5} = -40$ mV), which are both thermodynamically favorable for electron transfer to the b_D heme (18). However, the functional reasons of this stabilization remain to be established since, even if both one-electron redox potentials were exchanged (namely $E_{m,7.5}$ (MQH2/MSQ) $= -40$ mV and $E_{m,7.5}$ (MSQ/MQ) $= -150$ mV leading to $K_{S\ pH\ 7.5} \sim 10^{-2}$), they would be still favorable for electron transfer to heme b_D. Moreover, a high MSQ_D stability implies higher concentrations and possibly a longer life span for the semiquinone intermediate that however do not appear harmful for the bacterial cell as menaquinone is preferentially used during anaerobic respiration. In contrast, the lower stability of ubisemiquinone species in the bc_1 complex of aerobic organisms may have been natu-

rally selected to keep radical concentrations as low as possible, minimizing superoxide generation from O_2 with deleterious physiological consequences (51). To better understand the origin of the MSQ_D stability, its different possible protonation states should be taken into account. Additionally, other structural factors may drastically influence the radical stability, such as the presence of other ligands to the semiquinone: while an Asp and a Ser residue are hydrogen bonded to Q_i^-, a Lys residue (Lys-86) has been discussed as a potential additional hydrogen bond donor to MSQ_D (19, 20).

Role of the Lys-86 Residue—Using multifrequency ESEEM experiments, we did not find any evidence for the transfer of a measurable spin density on any other nucleus than that discussed above. Moreover, the ^{14}N ESEEM pattern is unchanged in the pH range from 6.5 to 8.5 (data not shown). This indicates that no additional direct hydrogen bond is formed between a nitrogen nucleus and MSQ_D in this pH range (Fig. 5). Interestingly, we have recently shown that the conserved residue Lys-86, located at the entrance of the Q_D site cavity is necessary for MSQ_D stabilization (19). Its substitution into Ala strongly reduces the quinol/nitrate oxidoreductase activity measured using various electron donors (19). Additionally, the inhibitory effect of PCP measured in the wild-type enzyme is strongly attenuated in this mutant (20). Given that the N_ζ of Lys-86 lies ~ 6 Å from the Cl_4 atom of the inhibitor, this raises the question of how Lys-86 is involved in the quinol oxidation mechanism by NarGHI. Using molecular modeling of the physiological substrate menaquinone in Q_D based on the PCP position, Bertero *et al.* (20) suggested that relatively small conformational movements of the Lys-86 side chain could occur and allow this residue to play a role in quinone stabilization, providing a direct hydrogen bond donor for the hydroxyl oxygen at position 4. Correct positioning of the quinol molecule within Q_D could be an essential function of Lys-86. Indeed, in the crystal structure of $NarGHI_{K86A}/PCP$, the inhibitor does not experience any polar contact with the protein, in particular with His-66, although it still binds to the enzyme. Moreover, the Q_D-binding pocket is largely preserved in this mutant form, as indicated by comparison of the $NarGHI_{K86A}$ three-dimensional structure with that of the wild-type enzyme (20).

Although the present work excludes a direct H-bond between O4 of MSQ_D and the N_ζ of Lys-86, it is possible that water molecules that are not resolved in the electron density map act as ligands to the menasemiquinone, as suggested for the ubiquinone bound to *E. coli* succinate dehydrogenase or for the menaquinone co-crystallized with *T. thermophilus* polysulfide reductase (47, 52). In this context, a water-mediated hydrogen bond between the N_ζ of Lys-86 and the O4 of MSQ_D could also occur (Fig. 5). Such a situation encountered in the Q_i binding site of the cytochrome bc_1 complex from the yeast *Saccharomyces cerevisiae* led to the absence of ^{14}N ESEEM modulation from the N_δ of His-202 in the intermediate ubisemiquinone state (42).

On the other hand, it should be kept in mind that several studies have reported on a dynamic behavior of quinone binding within Q sites. This could lead to different redox-dependent binding modes of the quinone during the quinol oxidation cycle. Such a phenomenon has been clearly evidenced for

ubiquinone in the Q_B quinone reduction site of *R. sphaeroides* photosynthetic reaction center: upon one-electron reduction, the ubisemiquinone radical undergoes a 4.5 Å (center to center) movement making a direct hydrogen bond to N_δ of His-190 that is not formed in the oxidized ubiquinone state (53). Recently, Horsefield *et al.* (54) proposed a reaction mechanism for the reduction of ubiquinone that involves a movement of ubiquinone between two different sites in the *E. coli* complex II.

The critical role of the Lys-86 residue for stabilizing MSQ_D and for proper NarGHI functioning could be caused by its ability to differently interact with the quinone species formed at the Q_D site during the quinol oxidation mechanism. In this context, a movement of the Lys-86 side chain could occur and could be associated to protonation/deprotonation events occurring during enzyme turnover allowing protons to be released to the periplasm. These could directly influence the stability of MSQ_D. A detailed study of the pH-dependence of MSQ_D redox properties and of the hydrogen bonding network to the radical will enable to characterize the protonation state of the radical, to better delineate the role of Lys-86, and to assess how deprotonation and oxidation events are coordinated during quinol oxidation by NarGHI. For this purpose, additional information about the exchangeable protons in hydrogen bonds can be provided by probing interactions with local magnetically coupled protons and the changes on substitution of ^2H_2O (18, 48, 55, 56). Such studies are currently being performed in our laboratories using high resolution EPR methods.

Concluding Remarks—Pulsed EPR experiments performed on *E. coli* membrane fractions containing overexpressed NarGHI provided direct evidence for nitrogen ligation to the natural menasemiquinone stabilized in the quinol oxidation site Q_D of the enzyme. S-band ESEEM/HYSCORE experiments enabled us to accurately determine the nuclear quadrupole interaction parameters of the interacting nitrogen nucleus and, thus, to assign the latter to the N_δ of a histidine residue hydrogen bonded to one of the semiquinone carbonyl groups. From the available structural data on the Q_D site, we propose that His-66, a b_D heme axial ligand, is the hydrogen-bonded nitrogen donor to the C1 oxygen whereas Lys-86 appears to be indirectly involved in MSQ_D stabilization, possibly via a water-mediated H-bond to the radical.

REFERENCES

1. Mitchell, P. (1979) *Science* **206,** 1148–1159
2. Jormakka, M., Byrne, B., and Iwata, S. (2003) *FEBS Lett.* **545,** 25–30
3. Wallace, B. J., and Young, I. G. (1977) *Biochim. Biophys. Acta* **461,** 84–100
4. Rothery, R. A., Bertero, M. G., Cammack, R., Palak, M., Blasco, F., Strynadka, N. C., and Weiner, J. H. (2004) *Biochemistry* **43,** 5324–5333
5. Lanciano, P., Savoyant, A., Grimaldi, S., Magalon, A., Guigliarelli, B., and Bertrand, P. (2007) *J. Phys. Chem. B.* **111,** 13632–13637
6. Guigliarelli, B., Magalon, A., Asso, M., Bertrand, P., Frixon, C., Giordano, G., and Blasco, F. (1996) *Biochemistry* **35,** 4828–4836
7. Bertero, M. G., Rothery, R. A., Palak, M., Hou, C., Lim, D., Blasco, F., Weiner, J. H., and Strynadka, N. C. (2003) *Nat. Struct. Biol.* **10,** 681–687
8. Blasco, F., Guigliarelli, B., Magalon, A., Asso, M., Giordano, G., and Rothery, R. A. (2001) *Cell Mol. Life Sci.* **58,** 179–193
9. Rothery, R. A., Blasco, F., Magalon, A., and Weiner, J. H. (2001) *J. Mol. Microbiol. Biotechnol.* **3,** 273–283
10. Giordani, R., Buc, J., Cornish-Bowden, A., and Cárdenas, M. L. (1997) *Eur. J. Biochem.* **250,** 567–577
11. Magalon, A., Rothery, R. A., Lemesle-Meunier, D., Frixon, C., Weiner, J. H., and Blasco, F. (1998) *J. Biol. Chem.* **273,** 10851–10856
12. Rothery, R. A., Blasco, F., Magalon, A., Asso, M., and Weiner, J. H. (1999) *Biochemistry* **38,** 12747–12757
13. Magalon, A., Rothery, R. A., Giordano, G., Blasco, F., and Weiner, J. H. (1997) *J. Bacteriol.* **179,** 5037–5045
14. Brito, F., DeMoss, J. A., and Dubourdieu, M. (1995) *J. Bacteriol.* **177,** 3728–3735
15. Morpeth, F. F., and Boxer, D. H. (1985) *Biochemistry* **24,** 40–46
16. Zhao, Z., Rothery, R. A., and Weiner, J. H. (2003) *Biochemistry* **42,** 5403–5413
17. Giordani, R., and Buc, J. (2004) *Eur. J. Biochem.* **271,** 2400–2407
18. Grimaldi, S., Lanciano, P., Bertrand, P., Blasco, F., and Guigliarelli, B. (2005) *Biochemistry* **44,** 1300–1308
19. Lanciano, P., Magalon, A., Bertrand, P., Guigliarelli, B., and Grimaldi, S. (2007) *Biochemistry* **46,** 5323–5329
20. Bertero, M. G., Rothery, R. A., Boroumand, N., Palak, M., Blasco, F., Ginet, N., Weiner, J. H., and Strynadka, N. C. (2005) *J. Biol. Chem.* **280,** 14836–14843
21. Hägerhäll, C., Magnitsky, S., Sled, V. D., Schröder, I., Gunsalus, R. P., Cecchini, G., and Ohnishi, T. (1999) *J. Biol. Chem.* **274,** 26157–26164
22. Ingledew, W. J., Ohnishi, T., and Salerno, J. C. (1995) *Eur. J. Biochem.* **227,** 903–908
23. Sato-Watanabe, M., Itoh, S., Mogi, T., Matsuura, K., Miyoshi, H., and Anraku, Y. (1995) *FEBS Lett.* **374,** 265–269
24. Lubitz, W., and Feher, G. (1999) *Appl. Magn. Reson.* **17,** 1–48
25. Deligiannakis, Y., Hanley, J., and Rutherford, A. W. (1999) *J. Am. Chem. Soc.* **121,** 7653–7664
26. Grimaldi, S., MacMillan, F., Ostermann, T., Ludwig, B., Michel, H., and Prisner, T. (2001) *Biochemistry* **40,** 1037–1043
27. Dikanov, S. A., Holland, J. T., Endeward, B., Kolling, D. R., Samoilova, R. I., Prisner, T. F., and Crofts, A. R. (2007) *J. Biol. Chem.* **282,** 25831–25841
28. Astashkin, A. V., Kawamori, A., Kodera, Y., Kuroiwa, S., and Akabori, K. (1995) *J. Chem. Phys.* **102,** 5583–5588
29. Peloquin, J. M., Tang, X. S., Diner, B. A., and Britt, R. D. (1999) *Biochemistry* **38,** 2057–2067
30. Bosch, M. K., Gast, P., Hoff, A. J., Spoyalov, A. P., and Tsvetkov, Y. D. (1995) *Chem. Phys. Letters* **239,** 306–312
31. Hanley, J., Deligiannakis, Y., MacMillan, F., Bottin, H., and Rutherford, A. W. (1997) *Biochemistry* **36,** 11543–11549
32. Lai, A., Flanagan, H. L., and Singel, D. J. (1988) *J. Chem. Phys.* **89,** 7161–7166
33. Flanagan, H. L., and Singel, D. J. (1987) *J. Chem. Phys.* **87,** 5606–5612
34. Lin, M. T., Samoilova, R. I., Gennis, R. B., and Dikanov, S. A. (2008) *J. Am. Chem. Soc.* **130,** 15768–15769
35. Lendzian, F., Rautter, J., Kaess, H., Gardiner, A. T., and Lubitz, W. (1996) *Ber Bunsenges Phys. Chem.* **100,** 2036–2040
36. Spoyalov, A. P., Hulsebosch, R. J., Shochat, S., Gast, P., and Hoff, A. J. (1996) *Chem. Phys. Letters* **263,** 715–720
37. Maniatis, T., Fritsch, E., and Sambrook, J. (1982) *Molecular Cloning: A Laboratory Manual,* Cold Spring Harbor, New York
38. Weber, A., Rohrer, M., Toerring, J. T., and Prisner, T. F. (1998) in *Proceedings of the 29th Congress AMPERE/13th ISMAR* (Ziessow, D., Lubitz, W., and Lendzian, F., ed) Vol. 2, p. 1138, International Society of Magnetic Resonance, Berlin
39. Schweiger, A., and Jeschke, G. (2001) *Principles of Pulse Electron Paramagnetic Resonance*, Oxford University Press, UK
40. Dikanov, S. A., and Tsvetkov, Y. D. (1992) *Electron Spin Echo Envelope Modulation (ESEEM) Spectroscopy*, CRC Press
41. Guigliarelli, B., Asso, M., More, C., Augier, V., Blasco, F., Pommier, J., Giordano, G., and Bertrand, P. (1992) *Eur. J. Biochem.* **207,** 61–68
42. Grimaldi, S. (2002) in *Doctoral Thesis, Chemistry Department,* J.-W. Goethe Universität, Frankfurt, Germany
43. Morton, J. R., and Preston, K. F. (1978) *J. Magn. Reson.* **30,** 577–582

44. MacMillan, F., Lendzian, F., and Lubitz, W. (1995) *Magn. Reson. Chem.* **33,** S81–S93

45. Grimaldi, S., Ostermann, T., Weiden, N., Mogi, T., Miyoshi, H., Ludwig, B., Michel, H., Prisner, T. F., and MacMillan, F. (2003) *Biochemistry* **42,** 5632–5639

46. Fritscher, J. (2004) *Phys. Chem. Chem. Phys.* **6,** 4950–4956

47. Jormakka, M., Yokoyama, K., Yano, T., Tamakoshi, M., Akimoto, S., Shimamura, T., Curmi, P., and Iwata, S. (2008) *Nat. Struct. Mol. Biol.* **15,** 730–737

48. Dikanov, S. A., Samoilova, R. I., Kolling, D. R., Holland, J. T., and Crofts, A. R. (2004) *J. Biol. Chem.* **279,** 15814–15823

49. Fritscher, J., Prisner, T. F., and MacMillan, F. (2006) *Appl. Magn. Reson.* **30,** 251–268

50. Robertson, D. E., Prince, R. C., Bowyer, J. R., Matsuura, K., Dutton, P. L., and Ohnishi, T. (1984) *J. Biol. Chem.* **259,** 1758–1763

51. Cape, J. L., Bowman, M. K., and Kramer, D. M. (2007) *Proc. Natl. Acad. Sci. U.S.A.* **104,** 7887–7892

52. Yankovskaya, V., Horsefield, R., Törnroth, S., Luna-Chavez, C., Miyoshi, H., Léger, C., Byrne, B., Cecchini, G., and Iwata, S. (2003) *Science* **299,** 700–704

53. Stowell, M. H., McPhillips, T. M., Rees, D. C., Soltis, S. M., Abresch, E., and Feher, G. (1997) *Science* **276,** 812–816

54. Horsefield, R., Yankovskaya, V., Sexton, G., Whittingham, W., Shiomi, K., Omura, S., Byrne, B., Cecchini, G., and Iwata, S. (2006) *J. Biol. Chem.* **281,** 7309–7316

55. Yap, L. L., Samoilova, R. I., Gennis, R. B., and Dikanov, S. A. (2006) *J. Biol. Chem.* **281,** 16879–16887

56. Flores, M., Isaacson, R., Abresch, E., Calvo, R., Lubitz, W., and Feher, G. (2007) *Biophys. J.* **92,** 671–682

57. Edmondson, D. T., and Speight, P. A. (1971) *Phys. Lett.* **34,** 325–326